J|A|C|S
ARTICLES

Published on Web 12/23/2010

# White-Light-Emitting Self-Assembled NanoFibers and Their Evidence by Microspectroscopy of Individual Objects

Carlo Giansante, Guillaume Raffy, Christian Schäfer, Hakim Rahma, Min-Tzu Kao, Alexandre G. L. Olive, and André Del Guerzo*

*Université Bordeaux 1, CNRS, Institut des Sciences Moléculaires, NEO Nanostructures Organiques, 351 crs de la Liberation, 33405 Talence cédex, France*

Received July 30, 2010; E-mail: a.del-guerzo@ism.u-bordeaux1.fr

***Abstract:*** The self-assembly of a blue-emitting light-harvesting organogelator and specifically designed highly fluorescent tetracenes yields nanofibers with tunable emissive properties. In particular, under near-UV excitation, white light emission is achieved in organogels and dry films of nanofibers. Confocal fluorescence microspectroscopy demonstrates that each individual nanofiber emits white light. A kinetic study shows that an energy transfer (ET) occurs between the blue-emitting anthracene derivative and the green- and red-emitting tetracenes, while inter-tetracene ETs also take place. Moreover, microscopy unravels that the nanofibers emit polarized emission in the blue spectral region, while at wavelengths higher than 500 nm the emission is not significantly polarized.

## Introduction

Self-assembly of chemical species by weak noncovalent interactions is a widespread strategy exploited by nature in its forms and functions[1] and is attracting considerable interest in the creation of artificial systems.[2] Self-assembly has, for example, brought significant advantages in the bottom-up approach to realize highly emissive multichromophoric nanostructures for light-harvesting and optoelectronic purposes.[3−5] Quasi-one-dimensional systems have also been attained by exploiting the programmed self-assembly of low-molecular-weight organic chromophores.[6,7] In the particular case of organogels, the heterogeneous soft material is composed of a removable fluid and a network of self-assembled nanofibers.[8] These fiber preparation methods exploiting solution processing are an alternative to vapor deposition of low-molecular-weight organic fluorophores[9] or electrospinning of molecular, macromolecular, or hybrid organic/inorganic constituents.[10−13] Interestingly, the latter multicomponent systems have been suggested as white-light-emitting materials, a property only rarely explored in organogels.[14−16] In all these cases[9−16] the bulk material composed of multiple components and of randomly dispersed nano- or micro-objects was investigated to characterize the emissive properties. Nevertheless, this resulted only in the determination of averaged macroscopic properties without full apprehension of the implications of heterogeneity and random orientations of objects. Besides, the influence of the anisotropic shape of the fibers on the emission of white light has not been studied so far, a feature that could be exploited in macroscopic materials. Thus, the particular characteristics of an *individual multicomponent* nanofiber have not been addressed yet. In this work we aimed to realize white-light-emitting self-assembled

(1) Cramer, F. *Chaos and Order*; Wiley-VCH: Weinheim, Germany, 1993.
(2) Lehn, J.-M. *Chem. Soc. Rev.* **2007**, *36*, 151.
(3) (a) Jonkheijm, P.; van der Schoot, P. P. A. M.; Schenning, A. P. H. J.; Meijer, E. W. *Science* **2006**, *313*, 80. (b) Hirschberg, J. H. K. K.; Brunsveld, L.; Ramzi, A.; Vekemans, J. A. J. M.; Sijbesma, R. P.; Meijer, E. W. *Nature* **2000**, *407*, 167. (c) Sijbesma, R. P.; Beijer, F. H.; Brunsveld, L.; Folmer, B. J. B.; Hirschberg, J. H. K. K.; Lange, J. H. K. K.; Lowe, J.K.; Meijer, E. W. *Science* **1997**, *278*, 1601.
(4) (a) Kaiser, T. E.; Stepanenko, V.; Würthner, F. *J. Am. Chem. Soc.* **2009**, *131*, 6719. (b) Kaiser, T. E.; Scheblykin, I. G.; Thomsson, D.; Würthner, F. *J. Phys. Chem. B* **2009**, *113*, 15836. (c) Zhang, X.; Rehm, S.; Safont-Sempere, M. M.; Würthner, F. *Nat. Chem.* **2009**, *1*, 623. (d) Uemura, S.; Sengupta, S,; Würthner, F. *Angew. Chem.* **2009**, *121*, 7965; *Angew. Chem., Int. Ed.* **2009**, *48*, 7825. (e) Zhao, Y. S.; Fu, H.; Peng, A.; Ma, Y.; Xiao, D.; Yao, J. *Adv. Mater.* **2008**, *20*, 2859. (f) Ajayaghosh, A.; Praveen, V. K. *Acc. Chem. Res.* **2007**, *40*, 644.
(5) (a) Zabala Ruiz, A.; Li, H.; Calzaferri, G. *Angew. Chem., Int. Ed.* **2006**, *118*, 5408. (b) Zabala Ruiz, A.; Li, H.; Calzaferri, G. *Angew. Chem., Int. Ed.* **2006**, *45*, 5282. (c) Ajayaghosh, A.; Praveen, V. K.; Vijayakumar, C. *Chem. Soc. Rev.* **2008**, *37*, 109.
(6) (a) Zang, L.; Che, Y.; Moore, J. S. *Acc. Chem. Res.* **2008**, *41*, 1596. (b) Würthner, F.; Bauer, C.; Stepanenko, V.; Yagai, S. *Adv. Mater.* **2008**, *20*, 1695. (c) Hoeben, F. J. M.; Jonkheijm, P.; Meijer, E. W.; Schenning, A. P. H. J. *Chem. Rev.* **2005**, *105*, 1491.
(7) For a comprehensive review on zero- and one-dimensional nanostructures based on low-molecular-weight organic chromophores see: Zhao, Y. S.; Fu, H.; Peng, A.; Ma, Y.; Xiao, D.; Yao, J. *Adv. Mater.* **2008**, *20*, 2859.
(8) (a) Terech, P.; Weiss, R. G. *Chem. Rev.* **1997**, *97*, 3133. (b) *Molecular Gels, Materials with Self-Assembled Fibrillar Networks*; Terech, P., Weiss, R. G., Eds.; Kluwer Press: Dordrecht, The Netherlands, 2005.
(9) (a) Zhao, Y. S.; Fu, H.; Peng, A.; Ma, Y.; Liao, Q.; Yao, J. *Acc. Chem. Res.* **2010**, *43*, 409. (b) Zhao, Y. S.; Fu, H.; Hu, F.; Peng, A.; Yang, W.; Yao, J. *Adv. Mater.* **2008**, *20*, 79.
(10) Ner, Y.; Grote, J. G.; Stuart, J. A.; Sotzing, G. A. *Angew. Chem., Int. Ed.* **2009**, *48*, 5143.
(11) Hou, Z.; Chai, R.; Zhang, M.; Zhang, C.; Cheng, P.; Xu, Z.; Li, G.; Liu, J. *Langmuir* **2009**, *25*, 12340.
(12) Chen, H.-C.; Wang, C.-T.; Liu, C.-L.; Liu, Y.-C.; Chen, W.-C. *J. Polym. Sci., Part B: Polym. Phys.* **2009**, *47*, 463.
(13) Vohra, V.; Calzaferri, G.; Destri, S.; Pasini, M.; Porzio, W.; Botta, C. *ACS Nano* **2010**, *4*, 1409.
(14) Yang, X.; Lu, R.; Xue, P.; Li, B.; Xu, D.; Xu, T.; Zhao, Y. *Langmuir* **2008**, *24*, 13730.
(15) Vijayakumar, C.; Praveen, V. K.; Ajayaghosh, A. *Adv. Mater.* **2009**, *21*, 2059.
(16) Abbel, R.; van der Weegen, R.; Pisula, W.; Surin, M.; Leclère, P.; Lazzaroni, R.; Meijer, E. W.; Schenning, A. P. H. J. *Chem.—Eur. J.* **2009**, *15*, 9737.


**10.1021/ja106807u** 

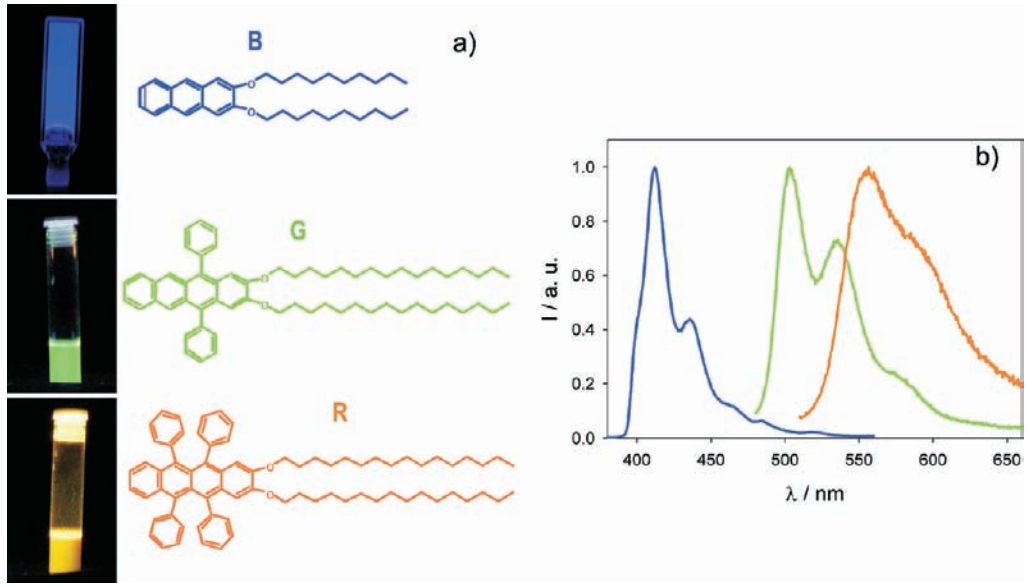


***Figure 1.*** (a) Pictures of a 2 mM **B** gel in DMSO, 10 $\mu$M **G** solution in THF, and 10 $\mu$M **R** solution in THF under UV light ($\lambda_{ex}$ = 365 nm) and the molecular structures. (b) Corrected fluorescence spectra of **B**, **G**, and **R** ($\lambda_{ex}$ = 365 nm).

nanofibers and ascertain by confocal fluorescence microspectroscopy[17] the spectral, photophysical, and anisotropic features of the individual nano-objects.

The above-mentioned optical properties are in general obtained by blending three to four components, for example, using molecules that display similar chemical structures and interact favorably in assembled multicomponent systems. This necessitates the use of a family of molecules with optical properties that can be tuned with small modifications of the structure. *n*-Acene derivatives are very good candidates as they can be tailored chemically, exhibit high fluorescence quantum yields, and record charge mobility in single crystals.[18] The HOMO−LUMO gap can be reduced by extending the $\pi$-conjugation along the long axis of the core by adding a conjugated aromatic ring or along the short axis with phenyl or alkynyltrialkylsilyl substituents. They constitute an alternative to oligo(phenylenevinylene), oligothiophene, perylene, or other fluorescent $\pi$-conjugated organogelators. In particular, the anthracene derivative **B** (2,3-bis(decyloxy)anthracene; Figure 1) displays a robust self-assembling ability in various organic solvents such as alcohols or DMSO,[19] even in the presence of organic or inorganic guests.[20,21] **B** differs by its particular packing through weak interactions excluding H-bonds, while displaying attractive emissive properties. In this work, the nanofibers of **B** are exploited as light-harvesting matrixes capable of hosting and sensitizing by excitation energy transfer[22] green and red emitters that have been specifically designed to be *co*-self-assembled with **B**. The photophysics and anisotropic properties of the three-component self-assembled nanofibers are revealed by optical microscopy.

## Results and Discussion

**Synthesis and Solution Properties of New Tetracenes.** As energy acceptors we have prepared new *n*-acenes that display red-shifted emission, high fluorescence quantum yields, and structural similarities to **B**. Thus, 2,3-bis(hexadecyloxy)-5,12-diphenyltetracene (**G**; Figure 1) and 2,3-bis(hexadecyloxy)-5,6,11,12-tetraphenyltetracene (**R**; Figure 1) have been synthesized. **G** and **R** were obtained by addition of phenylmagnesium bromide or phenyllithium to the 2,3-bis(hexadecyloxy)tetracene-5,12-dione and 2,3-bis(hexadecyloxy)-6,11-diphenyltetracene-5,12-dione derivatives, respectively, using hydriodic acid to promote final aromatization of the dihydroxy intermediates (Scheme 1). The dione precursors with hexadecyl chains were previously obtained by demethylation of the methoxy analogue[22,23] rapidly followed by a substitution reaction. In THF solutions, **G** and **R** show green ($\lambda_{em}$ = 502 nm) and orange-red ($\lambda_{em}$ = 555 nm) fluorescence with quantum yields reaching 53% and 69%, respectively (Table 1, Figure 1). The red shift relative to **B** is achieved using a tetracene core and the HOMO−LUMO gap is tuned with two or four phenyl substituents. These also raise the quantum yields as compared to those of 2,3-dialkoxytetracenes by reducing the singlet−triplet intersystem crossing, as previously described in other substituted *n*-acenes.[24]

(17) (a) Eisele, D. M.; Knoester, J.; Kirstein, S.; Rabe, J. P.; Van den Bout, D. A. *Nat. Nanotechnol.* **2009**, *4*, 658. (b) Lin, H.; Camacho, R.; Tian, Y.; Kaiser, T. E.; Würthner, F.; Scheblykin, I. G. *Nano Lett.* **2010**, *10*, 620. (c) Hoeben, F. J. M.; Shklyarevskiy, I. O.; Ponderoijen, M. J.; Engelkamp, H.; Schenning, A. P. H. J.; Christianen, P. C. M.; Maan, J. C.; Meijer, E. W. *Angew. Chem., Int. Ed.* **2005**, *45*, 1232. (d) Lang, E.; Sorokin, A.; Drechsler, M.; Malyukin, Y. V.; Köhler, J. *Nano Lett.* **2005**, *5*, 2635. (e) Hofkens, J.; Latterini, L.; Vanoppen, P.; Faes, H.; Jeuris, K.; De Feyter, S.; Kerimo, J.; Barbara, P. F.; De Schryver, F. C.; Rowan, A. E.; Nolte, R. J. M. *J. Phys. Chem. B* **1997**, *101*, 10588.
(18) (a) Anthony, J. F. *Angew. Chem., Int. Ed.* **2008**, *47*, 452. (b) Bendikov, M.; Wudl, F.; Perepichka, D. F. *Chem. Rev.* **2004**, *104*, 4891.
(19) (a) Desvergne, J.-P.; Brotin, T.; Meerschaut, D.; Clavier, G.; Placin, F.; Pozzo, J.-L.; Bouas-Laurent, H. *New J. Chem.* **2004**, *28*, 234. (b) Placin, F.; Desvergne, J.-P.; Lassègues, J.-C. *Chem. Mater.* **2001**, *13*, 117.
(20) Desvergne, J.-P.; Del Guerzo, A.; Bouas-Laurent, H.; Belin, C.; Reichwagen, J.; Hopf, H. *Pure Appl. Chem.* **2006**, *78*, 707.
(21) (a) Sangeetha, N. M.; Bhat, S.; Raffy, G.; Belin, C.; Loppinet-Serani, A.; Aymonier, C.; Terech, P.; Maitra, U.; Desvergne, J.-P.; Del Guerzo, A. *Chem. Mater.* **2009**, *21*, 3424. (b) Del Guerzo, A.; Olive, A. G. L.; Reichwagen, J.; Hopf, H.; Desvergne, J.-P. *J. Am. Chem. Soc.* **2005**, *127*, 17984.
(22) Reichwagen, J.; Hopf, H.; Del Guerzo, A.; Belin, C.; Desvergne, J.-P.; Bouas-Laurent, H. *Org. Lett.* **2005**, *7* (6), 971.
(23) Paraskar, A. S.; Reddy, A. R.; Patra, A.; Wijsboom, Y.-H.; Gidron, O.; Leitus, G.; Bendikov, M. *Chem.—Eur. J.* **2008**, *14*, 10639.
(24) Komfort, M.; Löhmannsröben, H.-G.; Salhammer, T. *J. Photochem. Photobiol., A* **1990**, *51*, 215.

***Scheme 1.*** Final Steps of the Synthesis of **G** and **R**[a]

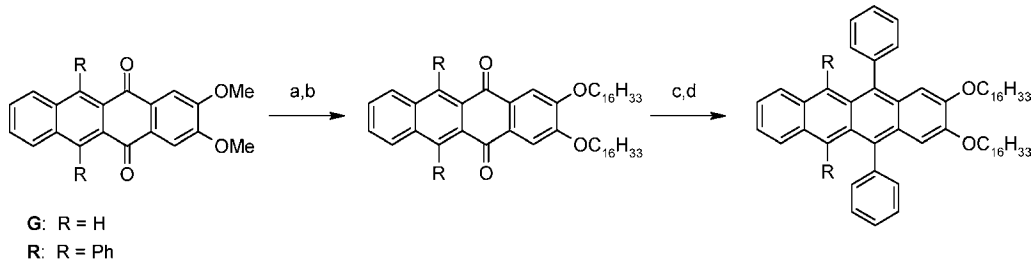


[a] Reagents and conditions: (a) $BBr_3$, DCM; (b) $K_2CO_3$, *n*-$C_{16}H_{33}Br$, DMF; (c) PhMgBr (for **G**) or PhLi (for **R**), THF; (d) HI, $Et_2O$.

***Table 1.*** Absorption and Emission Properties of **B**, **G**, and **R** in Solution and in Organogels (Deoxygenated): Lowest Energy Absorption Wavelength, $\lambda_{abs}$, Extinction Coefficient, $\varepsilon$, Emission Wavelength, $\lambda_{em}$, and Quantum Yield, $\Phi_{em}$, Decay Time, $\tau$, and Radiative Constant, $k_r$

| | solvent | $\lambda_{abs}$, nm | $\varepsilon \times 10^3$, $M^{-1}$ $cm^{-1}$ | $\lambda_{em}$, nm | $\tau$, ns | $k_r \times 10^7$, $ns^{-1}$ | $\Phi_{em}$ |
|---|---|---|---|---|---|---|---|
| **B** | THF | 366/376 | 7.0/4.8 | 389/410 | 5.0 | 5.0 | 0.25 |
| **G** | THF | 489 | 8.9 | 502 | 13.8 | 3.8 | 0.53 |
| **R** | THF | 523 | 9.6 | 555 | 13.6 | 5.1 | 0.69 |
| **B**-gel | DMSO | 385 | 7[b] | *c*/412 | *e* | | 0.24[f] |
| **B**-gel | MeOH | 385 | 7[b] | *c*/412 | *e* | | 0.08[f] |
| **W**-gel | DMSO | 385/488[a] | 7[b] | *d* | *e* | | 0.26[f] |
| **W**-gel | MeOH | 385/488[a] | 7[b] | *d* | *e* | | 0.11[f] |

[a] At 515−525 nm an additional shoulder is seen. [b] For $\varepsilon$ at 385 nm, the experimental error increases to ~15% due to high absorbance and excitation light diffusion. [c] Band around 389 nm not entirely measurable due to reabsorption (fluorimetry) and laser light scattering (microscopy). [d] White spectrum. [e] Multiexponential decays; see the text and Figure 6. [f] Excitation at 365 nm, measured using an integration sphere.

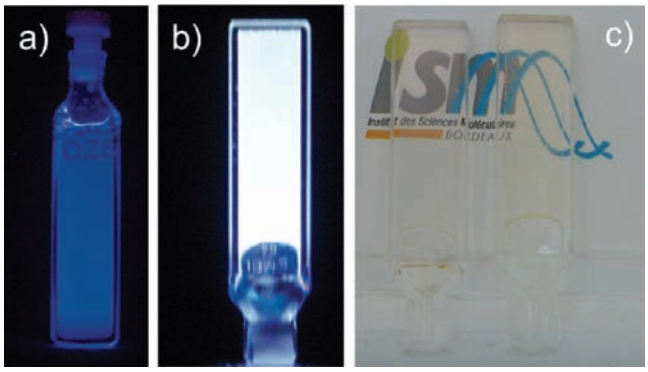


***Figure 2.*** (a, b) Pictures of cuvettes with 2.0 mM **B** with 0.012 equiv of **G** and **R** under UV light, $\lambda_{ex} = 365$ nm: (a) THF solution, (b) DMSO organogel (**W**-gel). (c) Pictures of quartz cuvettes containing pristine **B** organogel (**B**-gel) and **W**-gel under daylight (the logo of our institute can be seen in the background through the translucent gels).

**Spectroscopy of Gels.** Fluorescent nanofibers emitting blue light are obtained by gelating DMSO with **B**. This "**B**-gel" displays a structured emission spectrum and no undesired excimer-like emission (Figure 1, $\lambda_{ex} = 365$ nm, $\lambda_{em} = 412$ nm, $\Phi_{em} = 24\%$).[25] When both **G** and **R** are added in small quantities ($2.4 \times 10^{-5}$ M) to a $2.0 \times 10^{-3}$ M THF solution of **B**, only the latter emits (Figure 2a). In contrast, when a 120 °C hot DMSO solution of **B**, **G**, and **R** is air-cooled to room temperature, the three molecules self-assemble to form a translucent organogel (Figure 2c) with a melting temperature, $T_m$, of 37 °C (for **B**-gel $T_m = 38$ °C, Figure SI.2, Supporting Information). As a result, upon selective excitation of **B** with UV light, the blue emission decreases while those of **G** and **R** are observed. The partial excitation energy transfer from **B** to the energy acceptors can be modulated by changing the concentration of the acceptors, and using 0.012 equiv of **G** and **R**, a white-light-emitting "**W**-gel" is obtained (Figure 2b). Indeed, the emission mostly consists of the addition of the spectral features of the **B**-gel and of slightly narrowed and 2 nm red-shifted spectra of **G** and **R** (Figure 3). This slight band narrowing is reminiscent of emitters confined in a lattice with a high degree of orientation and a reduced vibrational degree of freedom, as well as more alike energy levels.[26] Only the near-UV emission is partly reabsorbed by the gel that is translucent to visible light (see Figure 2c). The corresponding CIE 1931 chromaticity coordinates for a two-degree field of view ($x = 0.319$, $y = 0.332$; Figure 3b) nearly match those of the most common white light standard (daylight simulator D65, $x = 0.31292$, $y = 0.32933$). In addition, the fluorescence quantum yield[25] of the **W**-gel reaches 26%, indicating the low loss of excited states in the gel. Interestingly, while a **W**-gel can be obtained also using another solvent, some of the spectral properties change. Indeed, when methanol is gelled by **B**, **G**, and **R** in adequate proportions, although the spectrum shows slightly more **G** and less **R** emission (Figure 3a), white light is obtained (0.012 equiv of **G** and **R**, CIE $x = 0.306$, $y = 0.331$). Besides, the quantum yield is lower ($\Phi_{em} = 11\%$), in accordance with the fact that the **B**-gel of MeOH emits less than the **B**-gel of DMSO ($\Phi_{em} = 8\%$ vs 24%, Table 1). It has to be noticed that previous studies by small-angle X-ray scattering had shown that **B**-gels of DMSO show a high degree of crystallinity,[27] while no intense scattering for MeOH gels has been reported.

**Spectroscopy of Individual Nanofibers.** Spatial, spectral, and temporal resolution is achieved by confocal fluorescence

(25) Quantum yields $\Phi_{em}$ of gels measured using an integrating sphere according to the following:(a) Pålsson, L.-O.; Monkman, A. P. *Adv. Mater.* **2002**, *14*, 757. (b) Porrès, L.; Holland, A.; Pålsson, L.-O.; Monkman, A. P.; Kemp, C.; Beeby, J. *J. Fluoresc.* **2006**, *16*, 267. Quantum yields $\Phi_{em}$ in solution using as a reference fluorescein at pH 11 according to the following: Crosby, G. A.; Demas, J. N. *J. Phys. Chem.* **1971**, *75*, 991.

(26) Bloess, A.; Durand, Y.; Matsushita, M.; Verbeck, R.; Groenen, E. J. J.; Schmidt, J. *J. Phys. Chem. A* **2001**, *105*, 3016.

(27) Terech, P.; Aymonier, C.; Loppinet-Serani, A.; Bhat, S.; Banerjee, S.; Das, R. K.; Maitra, U.; Del Guerzo, A.; Desvergne, J.-P. *J. Phys. Chem. B* **2010**, *114*, 11409.

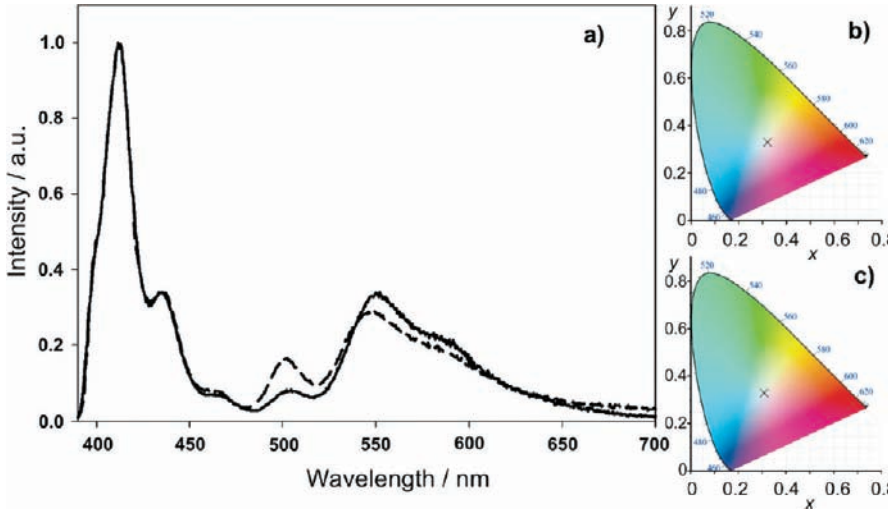


***Figure 3.*** (a) Corrected fluorescence spectra ($\lambda_{ex}$ = 365 nm) of (full line) a **W**-gel/DMSO and (dashed line) a **W**-gel/MeOH. (b) CIE 1931 chromaticity coordinates of **W**-gel/DMSO: $x = 0.319$, $y = 0.332$. (c) CIE 1931 chromaticity coordinates of **W**-gel/MeOH: $x = 0.306$, $y = 0.331$.

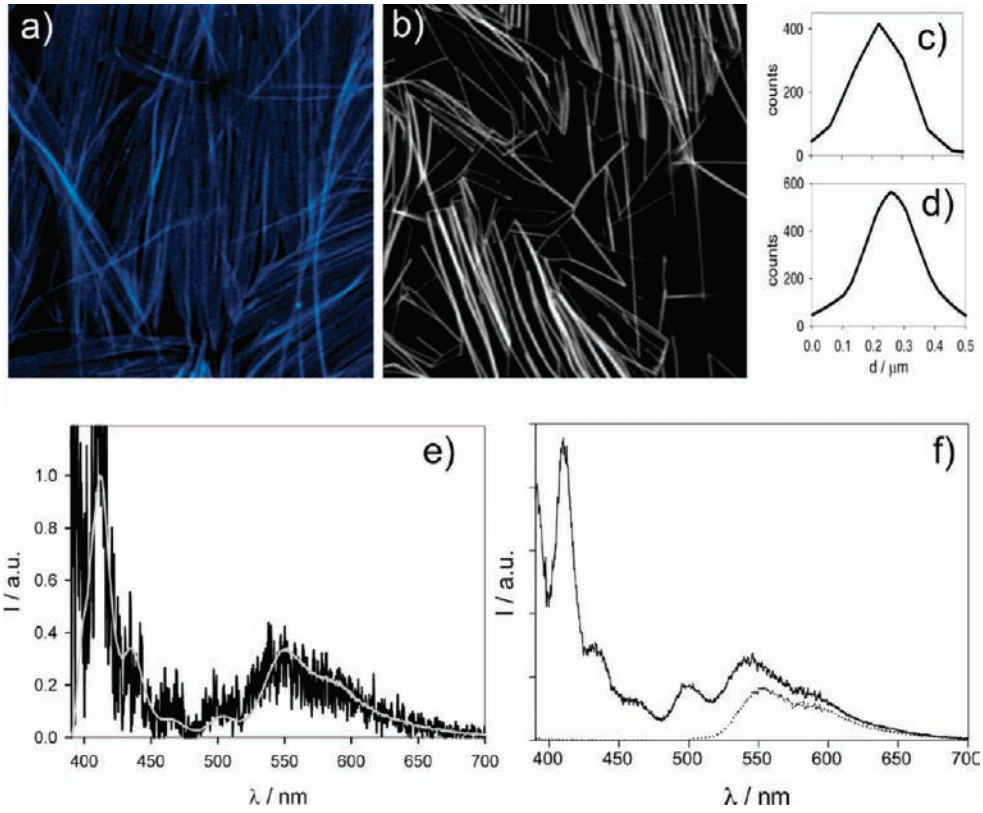


***Figure 4.*** (a−d) $\lambda_{ex}$ = 385 nm, $\lambda_{em}$ > 405 nm: (a, b) fluorescence intensity confocal microscopy image (30 × 30 $\mu$m, 80 × 80 nm/pixel) and (c, d) typical intensity profile of a fiber of (a, c) a **B**-gel and (b, d) a **W**-gel of DMSO at 22 °C. (e) Intensity-corrected fluorescence spectrum of a 5 $\mu$m × 200 nm portion of the **W**-gel ($\lambda_{ex}$ = 385 nm; see ref 29). For comparison, the same spectrum as Figure 3a is drawn in gray (intensities matched, au). (f) Intensity-corrected fluorescence spectra integrated over a 10 × 10 $\mu$m area of a **W**-gel: (full line) $\lambda_{ex}$ 385 = nm, (dashed line) $\lambda_{ex}$ = 488 nm, $\lambda_{em}$ > 500 nm.

microscopy and is used to characterize the origin of the white light emission. The deoxygenated solvated **W**-gel and **B**-gel using the less volatile solvent DMSO are formed directly on a cover glass, while the transfer of a three-component MeOH gel was less successful. Unless otherwise specified, all the **B**-gels and **W**-gels described below are obtained from degassed DMSO under continuous nitrogen flow to limit the photobleaching due to oxygen. At close proximity of the glass−gel interface, emissive three-dimensional fiber networks surrounded by a nonemissive bulk are observed. The networks are undistinguishable (Figure 4a,c), and the optical diffraction-limited cross-section of the fibers is typically ∼200 nm, while some larger fiber bundles of widths within ∼500 nm are less frequently observed. These quite homogeneous and long fibers distribute randomly or form domains tens of micrometers in diameter of partially aligned fibers, but do not form big amorphous aggregates. These nanofiber networks are very similar to that of **B**-gels previously characterized by electron microscopy displaying fibers 80−200 nm and bundles 0.5−1 $\mu$m wide.[19b] A model has been proposed in which **B** molecules are assembled

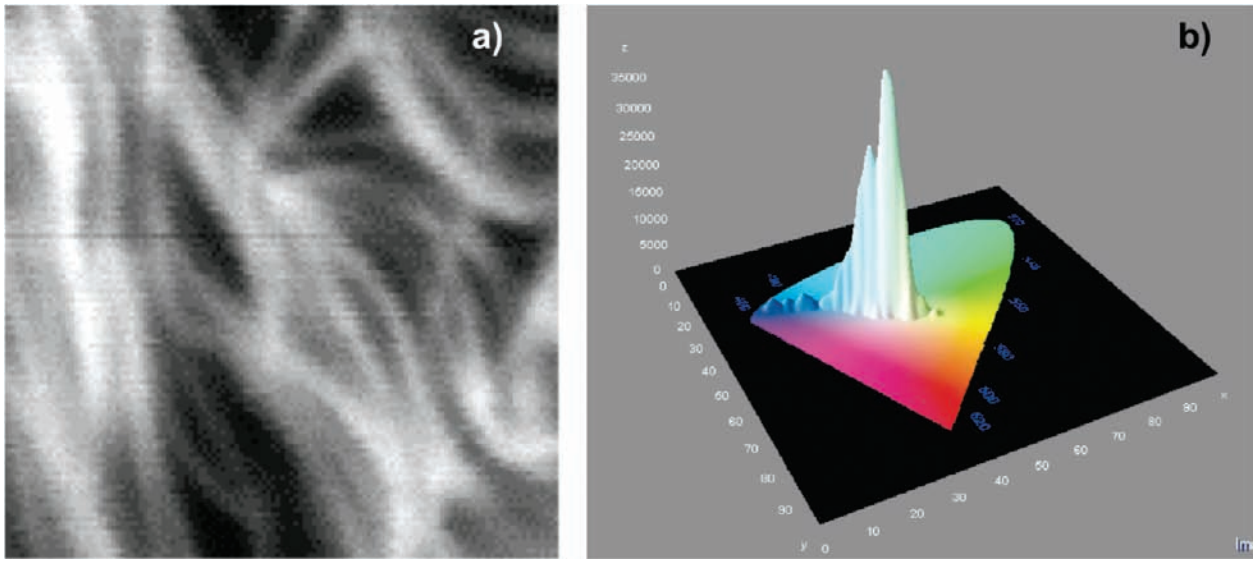


***Figure 5.*** (a) Fluorescence intensity confocal microscopy image (20 × 20 $\mu$m) of a **W**-gel (DMSO) at 22 °C ($\lambda_{ex}$ = 385 nm, $\lambda_{em}$ > 405 nm). (b) Distribution of the CIE 1931 chromaticity coordinates of 500 fluorescence spectra, similar to Figure 4a, acquired while scanning the nanofibers in an area of 20 × 20 $\mu$m. The *z*-scale represents the number of photons yielding the given coordinates.

into coaxial triads, stacked head-to-tail into sheets forming the fibers (see Figure SI.3, Supporting Information).[28] X-ray and neutron scattering studies have confirmed a hexagonal molecular packing of **B** in organo- and aerogels,[27] in agreement with the crystal structures of the model analogues ($P\bar{3}$ and $R\bar{3}$ space groups[28]). In **W**-gels, **G** and **R** do thus not significantly alter the nanostructures induced by **B**, in line with the expectations arising from an alkyloxy substitution of all three components in positions 2 and 3.[21] The following studies support this statement (vide infra).

Fluorescence microspectroscopy reveals that the **W**-gel is composed of white-light-emitting self-assembled nanofibers (**W**-SANFs). Indeed, the spectra of individual **W**-SANFs under near-UV excitation ($\lambda_{ex}$ = 385 nm) are very similar to those of the bulk (Figure 4e,f). Figure 4e shows a typical spectrum obtained accumulating light emitted from a 5 $\mu$m × 200 nm line, the equivalent of a segment of an individual isolated **W**-SANF.[29] A statistical analysis on 500 such segments within a **W**-gel (Figure 5a) reveals that the occurrence of colors (Figure 5b) is peaking in the white light coordinate region and is moderately distributed in the "off-white" light areas. The color coordinates fluctuate mostly on a line connecting those of the **B** component and those of the **G**/**R** mixture. This shows that the nanofibers behave like a two-component system, with slightly varying contributions of **B** and of the **G**/**R** mixture. This also shows that **G** and **R** are quite homogeneously dispersed in the **B** light-harvesting matrix.

**Photophysics within Individual Nanofibers.** The key process that contributes to achievement of white light emission in **W**-SANFs is a partial excitation energy transfer (ET) from the light-harvesting matrix **B** to the energy acceptors **G** and **R**. The spectral overlaps for Förster-type resonant energy transfer are sufficiently large for energy transfers on the nanometer scale, with values of $J_{BG} = 1.5 \times 10^{14}$ $M^{-1}cm^{-1}$ $nm^4$ between **B** and **G** and $J_{BR} = 1.2 \times 10^{14}$ $M^{-1}cm^{-1}$ $nm^4$ between **B** and **R**. Time-resolved confocal fluorescence lifetime imaging microscopy (FLIM) for **B** emission (400 nm < $\lambda_{em}$ < 450 nm) in **B**- and **W**-SANFs reveals complex excited-state decays that can be represented by triexponential functions. The decay times, $\tau$, are significantly shorter in **W**-SANFs than in **B**-SANFs (Figure 6c), with a distribution of values essentially around weighted means of 3.1 and 4.9 ns, respectively. Besides, the cumulated fluorescence of **G** and **R** in the **W**-SANFs rises with time upon selective excitation of **B** with a distribution of $\tau$ around a weighted mean value of 3.5 ns ($\lambda_{ex}$ = 385 nm, $\lambda_{em}$ > 500 nm; Figure 6e′,f). Their emission decay occurs at a longer time scale with the same decay time as when **G** and **R** are directly excited ($\tau$ = 15 ns, $\lambda_{ex}$ = 488 nm; compare parts d, e″, and f of Figure 6). The concurrent quenching of **B** and emission rise for **G** and **R** on comparable time scales (Figure 6b,e′) clearly indicates an excitation energy transfer taking place from **B** to **G** and **R** upon selective excitation of **B**.[29] Moreover, at $\lambda_{ex}$ = 488 nm both **G** and **R** can absorb, but the emission reflects exclusively the spectral features of **R** (Figure 4f), suggesting a hetero-ET, **G** → **R** ($J_{GR} = 3.8 \times 10^{14}$ $M^{-1}cm^{-1}$ $nm^4$). The unambiguous determination of the relative contributions of **B** → **G**, **B** → **R**, and **G** → **R** hetero-ETs (see the spectral overlaps, Figure SI.4, Supporting Information) requires a more detailed study that is beyond the scope of this paper, but their occurrence is confirmed by the results presented below. The overall **B** to acceptors transfer is efficient in the **W**-gel with an average estimate of the energy transfer kinetics obtained from the lifetime distributions of $\langle k_{ET} \rangle = 1.2 \times 10^8$ $s^{-1}$. Within the doping range used (2.4% in total), no large phase separation and inhomogeneous acceptor dispersion is favored, as confirmed by quite homogeneous FLIM images.

**Polarization Microscopy of Individual Nanofibers.** The particular interest in using anisotropic nano-objects is confirmed on individual fibers by confocal fluorescence polarization (*P*) imaging under linearly polarized laser excitation. Molecules selectively absorb linearly polarized light when their absorption

(28) Olive, A. G. L.; Raffy, G.; Alouchi, H.; Léger, J.-M.; Del Guerzo, A.; Desvergne, J.-P. *Langmuir* **2009**, *25*, 8606.

(29) Each spectrum results from 20 pixels taken every 250 nm and is corrected for instrumental response. Selective excitation of **B** at $\lambda_{ex}$ = 385 nm in **W**-SANFs is achieved since **B** absorbs at least 100 times more than **G** or **R**. At $\lambda_{ex}$ = 488 nm, both **G** and **R** are excited, and two-photon excitation of **B** has been ruled out experimentally. An excitation wavelength of 490 nm < $\lambda_{ex}$ < 700 nm is not available.

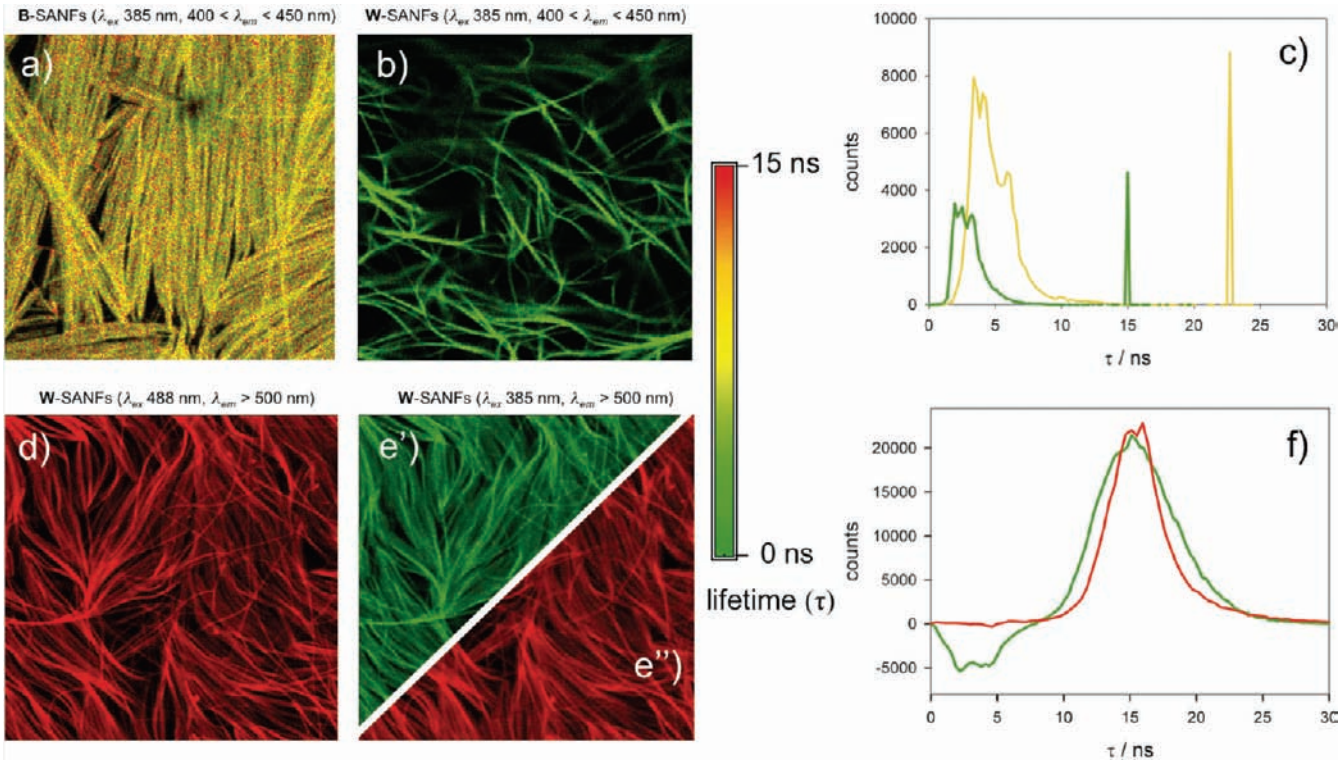


***Figure 6.*** (a, b, d, e) Confocal FLIM images (30 × 30 $\mu$m) with color codes green, yellow, and red representing average decay times from shorter to longer: (a) **B**-gel, (b, d, e) **W**-gel, (a, b) $\lambda_{ex} = 385$ nm, 400 nm < $\lambda_{em}$ < 450 nm, (d) $\lambda_{ex} = 488$ nm, $\lambda_{em} > 500$ nm, (e′, e″) $\lambda_{ex} = 385$ nm, $\lambda_{em} > 500$ nm, (e′) rise, (e″) decay. (c) Histograms of decay time $\tau$ distributions obtained by triexponential fitting of decays of (yellow) image a and (green) image b. (f) $\tau$ distributions obtained by (red) exponential fitting of decays of image d and (green) biexponential fitting of transient emission of image e. Decay = positive, and rise = negative.

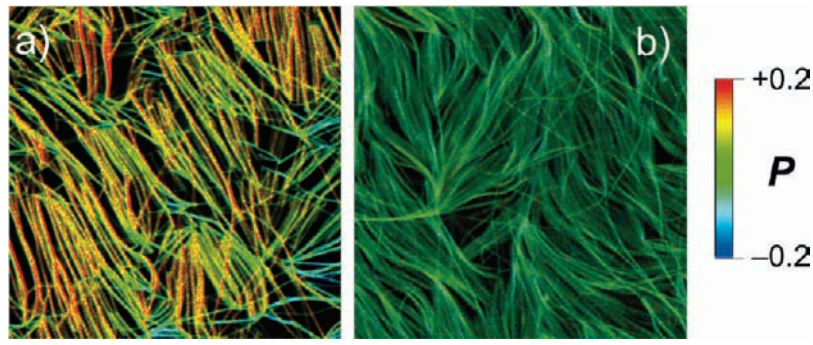


***Figure 7.*** Fluorescence polarization confocal images (30 × 30 $\mu$m) under horizontally polarized excitation (east/west, $\lambda_{ex} = 385$ nm) of a **W**-gel: (a) 400 nm < $\lambda_{em}$ < 450 nm, (b) $\lambda_{em} > 500$ nm. Color codes correspond to the polarization *P*: from negative to positive, blue, green, and red.

dipole, which in **B**, **G**, and **R** is along the short molecular axis, is oriented parallel to the axis of the excitation beam (photoselection). The resulting emission, stemming from the same dipolar transition, is characterized by the polarization *P*, calculated at each image pixel using the following equation:

$$P = \frac{I_{\parallel} - I_{\perp}}{I_{\parallel} + I_{\perp}} \qquad (1)$$

where $I_{\parallel}$ is the intensity of linearly polarized emission measured parallel to the excitation beam and $I_{\perp}$ is the intensity of polarized emission measured on the perpendicular axis. *P* can vary from −1 to +1 and with the angle $\theta$ of the nanofiber with respect to the orientation of the laser beam polarization. Indeed, a strong variation of *P* vs $\theta$ reveals a preferential orientation of the molecules within the nanofiber, while $P \approx 0$ (overall depolarization) and $P < 0$ (change of orientation of the polarization) indicate homo- or heteromolecular ETs.

In **W**-SANFs the **B** component emits light moderately polarized perpendicular to the long axis of the fibers (400 nm < $\lambda_{em}$ < 450 nm). In our experimental setup, this corresponds to a positively polarized emission with $P = 0.25$ for north/south fibers that display an angle of $\theta = 90 \pm 5°$ relative to the laser polarization (Figure 7a, red color code) and a negative polarization for east/west fibers ($P = -0.10$, blue, $\theta = 0 \pm 5°$). The polarization varies monotonously between these two extremes when the fibers are oriented with an intermediate angle $\theta$ (Figure 8a), as expected for a set of fibers displaying the same emission.[30] The occurrence of polarized emission changing strongly with the angle $\theta$ indicates a high degree of molecular

(30) A quantitative analysis of *P*, beyond our scope, requires taking into account molecular packing, effects of the substrate, and optics.

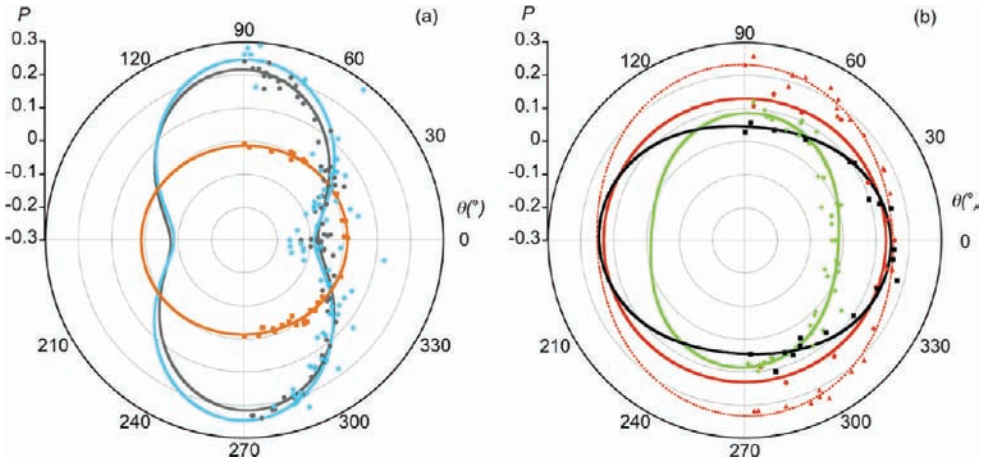


***Figure 8.*** Polar plots of average $P$ for individually picked SANF segments (2−5 $\mu$m long) as a function of the angle $\theta$ of the fiber axis with respect to the laser polarization (east/west): (a) $\lambda_{ex} = 385$ nm, (gray circles) **B**-SANFs, $\lambda_{em} > 405$ nm, (blue circles) **W**-SANFs, 400 nm $< \lambda_{em} <$ 450 nm, (orange squares) $\lambda_{em} > 500$ nm; (b) $\lambda_{ex} = 488$ nm, $\lambda_{em} > 500$ nm, (black squares) **W**-SANFs, (green tilted squares) **B** + **G** (1.2%), (full red circles) **B** + **R** (1.2%), (red triangles) **B** + **R** (0.05%). Full lines are guides to the eye only and are obtained by fitting $P$ with a simple sinusoidal function.

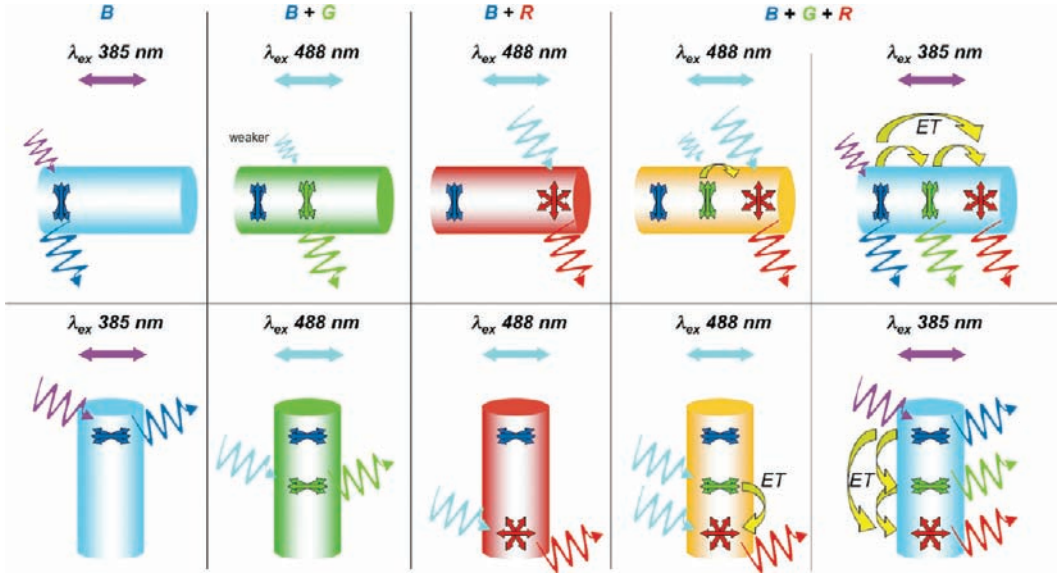


***Figure 9.*** Schematic representation of some photophysical processes in **B**-, **BR**-, **BG**-, and **W**-gels: (top) east/west fibers, (bottom) north/south fibers. Wavy arrows represent absorbed and emitted colors. Double arrows represent the polarization of the excitation and of the emission, as determined in the latter by the orientation of the molecules. Multiple arrows schematically suggest that several orientations are possible: for example, in **B**-gel the **B** molecules emit blue light preferentially perpendicular to the fiber axis, while in **BR**-gel **R** emission is on average more random. Yellow arrows represent energy transfer. In east/west fibers of **BG**- and **W**-gels, **G** absorbs 488 nm light less efficiently than **R** (the orientation of the **G** dipole and polarization of excitation match less). See the text.

order and a preferential average orientation of the **B** molecules within the **W**-SANFs. The results are very similar to those obtained for **B**-SANFs (Figure 8a, $-0.08 \le P \le +0.22$), further confirming that the self-assembly of **B** is not affected by the presence of both **G** and **R**. Besides, an important contribution to the generation of negative $P$ values could be the partial rotation of the emission polarization after excitation by an efficient exciton hopping processes, i.e., **B** → **B** donor−donor excitation energy transfers shown to occur in organogels[31] and J-aggregates.[17b] In contrast, the fluorescence arising from the **G** and **R** components in the **W**-SANFs is almost not polarized when sensitized by **B** ($\lambda_{ex} = 385$ nm, $\lambda_{em} > 500$ nm, Figure 8a).[32]

To gain further insight into the polarized emission of the acceptors within the nanofibers, we have also excited gels at 488 nm, a wavelength at which only **G** and **R** can absorb, and measured $P$ of the resulting emission ($\lambda_{em} > 500$ nm; see the spectrum in Figure 4f). The results are not as clear-cut as under UV excitation, but interesting indications on the tetracenes can be deduced. Figure 8b shows the polarization plots for a **W**-gel, a gel of **B** with only **R** (**BR**-gel), and a gel of **B** with only **G** (**BG**-gel). Figure 9 is a schematic representation of some of the photophysical processes occurring in these SANFs and can be used as a simplified guide. For the **BR**-gel, two cases are examined with 0.05% or 1.2% **R**. When **R** is diluted into **B** at 0.05% and excited directly, it emits always with a positive $P$ almost independently of the orientation $\theta$ of the SANF,

(31) (a) Ajayaghosh, A.; Praveen, V. K.; Vijayakumar, C.; George, S. J. *Angew. Chem., Int. Ed.* **2007**, *46*, 6260. (b) Herz, L. M.; Daniel, C.; Silva, C.; Hoeben, F. J. M.; Schenning, A. P. H. J.; Meijer, E. W.; Friend, R. H.; Phillips, R. T. *Phys. Rev. B* **2003**, *68*, 045203.

(32) Arithmetically estimated, depending on the polarization of the detected light, the emitted "off-white" light should vary between a yellow tone (CIE 0.33, 0.35) and a blue tone (CIE 0.30, 0.30).

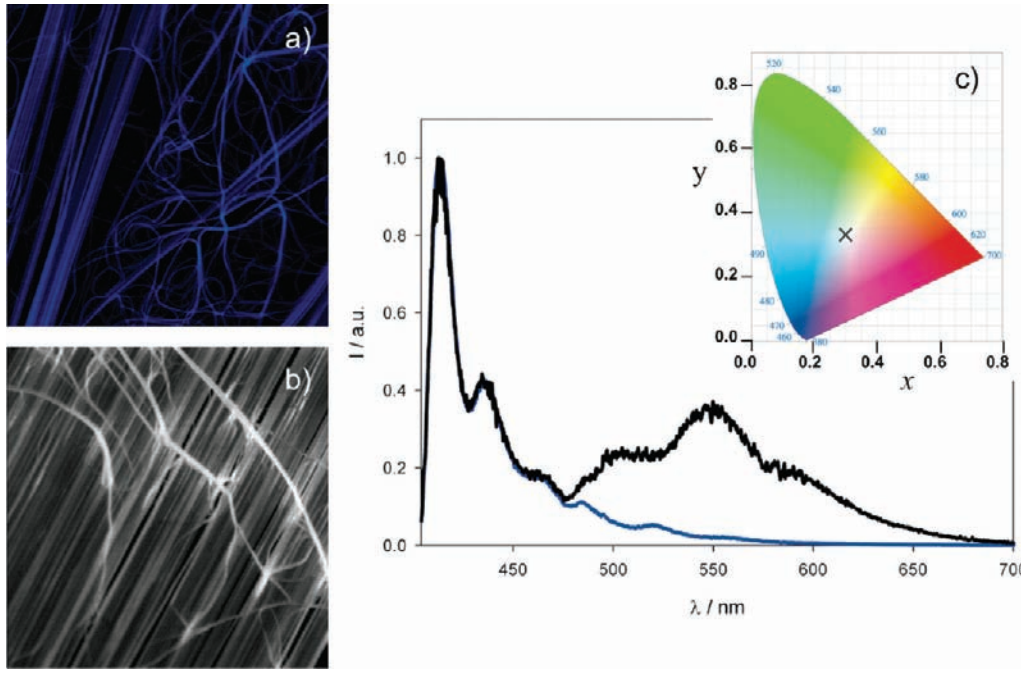


***Figure 10.*** (a, b) Fluorescence intensity confocal microscopy image (65 × 65 $\mu$m, 127 × 127 nm/pixel) of a dry SANF network obtained by drop-casting of a deoxygenated 0.1 mM **B**/DCM solution (a) without and (b) with 25 and 75 $\mu$M **G** and **R**, respectively, at 22 °C ($\lambda_{ex}$ = 385 nm, $\lambda_{em}$ > 405 nm). (c) Corrected fluorescence spectra collected on (blue line) area a and (black line) area b (intensities (au) are matched). The inset shows the CIE 1931 chromaticity coordinates corresponding to area b: $x = 0.29$, $y = 0.33$.

indicating multiple (or random) orientations of **R** molecules in the fiber and the absence of strong depolarization processes. When **R** is present at a higher concentration of 1.2%, $P$ is also positive but with lower values ($P \approx 0.13$), suggesting a partial concentration-dependent depolarization of **R** emission due to a homo-ET, **R** → **R**. This ET most probably results from a resonant Förster-type interaction which is disfavored in the **B** + 0.05% **R** gel due to the higher dilution and distance between the chromophores. A low $P$ value ($P < 0.1$) is also observed when a 1.2% concentration of only **G** is mixed with **B**, suggesting also that a **G** → **G** ET is present. In this case, however, the variation of $P$ with $\theta$ indicates that **G** molecules are preferentially oriented like the **B** molecules in the **B**-gel. The emission polarization in **W**-SANFs with 1.2% **G** and **R** results from the combination of several effects. As mentioned previously, at $\lambda_{ex}$ = 488 nm the emission stems exclusively from **R** (Figure 4f). For east/west fibers ($\theta \approx 0°$), the emission and $P$ value of the **W**-SANF are similar to those of a **BR**-SANF, suggesting that the emission of **R** results essentially from the direct excitation of **R** and negligibly from a **G** → **R** sensitization. In contrast, for north/south fibers ($\theta \approx 90°$) the $P$ values are almost reduced to zero. In this case, we suggest that **R** is excited not only by direct absorption of the laser light, but also due to **G** → **R** sensitization. Because multiple energy transfers occur (**G** → **G**, **G** → **R**, and **R** → **R**) and the **R** molecules are randomly oriented, the emission of **R** is almost totally depolarized. The difference between these two cases is due to a photoselection that affects **G** (preferentially oriented, selectively absorbs) and not **R** (more randomly oriented, always absorbs). In the **W**-SANFs, upon excitation of **B** at $\lambda_{ex}$ = 385 nm, the emission of **G** + **R** is observed and the overall polarization is close to zero for each angle $\theta$. In this case, **G** and **R** are both excited by **B** → **G** and **B** → **R** ETs, and in addition intra-acceptor ETs can occur (**G** → **R**, **G** → **G**, and **R** → **R**). The combination of the efficient **B** → **B** exciton hopping, the previously mentioned ETs, and the lack of preferential orientation of **R** results in an absence of overall polarization of the **G** + **R** emission.

**Dry Films of Nanofibers.** To determine whether desolvated SANFs present the same properties as the solvated SANFs, we have prepared films on a surface by depositing a solution of **B**, **G**, and **R** on a glass slide using a volatile solvent that does not lead to bulk gelification of **B**. The formation of nanofibers directly on the surface is observed by microscopy after rapid evaporation of the dichloromethane solvent (Figure 10), although only dilute solutions of **B** (0.10 mM), **G** (25 $\mu$M), and **R** (75 $\mu$M) have initially been used. The concentration at which fibers are formed during solvent evaporation could not be determined, but it is expected that fiber formation and blending of the three components occur at a concentration higher than in the case of DMSO gels. Microspectroscopy reveals that these **W**-SANFs also emit white light, as shown in Figure 10, when using doping percentages of **G** (0.25 equiv) and **R** (0.75 equiv). This result suggests that the overall energy transfer process and/or that the blending of the acceptors within the nanofibers are less efficient in this case.[33] Interestingly, we have also observed that on many parts of the film the fibers spontaneously align on areas surpassing 100 $\mu m^2$.

## General Discussion and Conclusion

The organogels composed of **B**, **G**, and **R** yield color-tunable fluorescent fibers, with spectral features varying with the proportions of the three components, as well as the wavelength of irradiation. At a composition of 1.2% **G** and 1.2% **R**, while only **R** fluorescence occurs when exciting at 488 nm, the three components all emit when irradiating at 385 nm. The light-harvesting and blue-emitting anthracene matrix sensitizes the green and red tetracene acceptors by the partial energy transfer processes **B** → **G** and **B** → **R**. According to the spectral overlap values, **G** should be more sensitized than **R**, although with the

additional **G** → **R** ET white light emission is achieved. The microspectroscopy studies have revealed that all the nanofibers individually emit white light and that the photophysical properties are similar in all the fibers. The tetracenes are homogeneously dispersed into or onto the fibers, as shown by optical microscopy, although the polarization studies reveal that while **B** and **G** display a similar preferential orientation, **R** is more randomly oriented. Two molecular characteristics distinguish **B**, **G**, and **R**. First, the alkyl chains of the tetracenes are slightly longer than those of **B**, and second, the phenyl substitutions of the tetracenes are bulky. The phenyls can disfavor the insertion of the tetracenes into the tightly packed **B** matrix, in which anthracene cores interact closely along their unsubstituted edges (see Figure SI.3, Supporting Information) and in which it has been shown previously that tetracenes without substitutions on the edges integrate more efficiently.[21] This effect is more pronounced for the bulky **R**, which could thus have a tendency to partially self-aggregate or even interact on the outskirts of the fibers. Interestingly, the resulting energy transfer is still efficient with a small doping ratio, and only the polarization of the emission at $\lambda_{em} > 500$ nm is influenced. The high degree of order at the molecular level of the **B** constituent in the nanofibers[26,27] is not perturbed and is important, as it constitutes the basis for a robust self-assembly, induces a polarized blue emission, and favors a **B** → **B** exciton hopping that could contribute to the light-harvesting process. The organization of the self-assembly is also influenced by the solvent. Indeed, the high quantum yields of emission measured in **B**- and **W**-gels of DMSO can be related to the partial crystallinity[27] of the self-assembly and the resulting reduction of defect-induced quenching processes. In the case of the dried fibers, it can be furthermore suggested that the blending of the three components into SANFs is affected by the conditions in which the self-assembly occurs. In particular, the temperature is lower, the critical concentration is higher, and the surface can influence the fiber growth, also inducing a very interesting self-alignment process. Only very recently a similar alignment has been observed for another gel on mica and attributed to epitaxial self-assembly.[34]

In conclusion, using microspectroscopy, this work has shown that self-assembly is an efficient method to accurately blend three components into highly organized and anisotropic nano-objects. Original perspectives could derive from the use of individual white-light-emitting nanofibers and can also be deduced from the observation that self-assembled nanofibers are adapted for the preparation of desolvated thin films[34,35] or aerogels,[21] for macroscopic alignment yielding highly organized materials,[36] or for semiconductivity.[34]

## Experimental Section

**Synthesis. 1. General Procedures.** 2,3-Bis(decyloxy)anthracene as well as the precursors for the green and red compounds were synthesized following literature procedures.[22,23] All solvents and chemicals were commercially available and used without further purification unless otherwise stated. THF was distilled over sodium prior to use. NMR spectra were recorded on a 300 MHz NMR spectrometer (Bruker, Advance 300), and HRMS measurements were performed using a QStar mass spectrometer (Applied Biosystems) equipped with an ESI source and a time-of-flight detector.

**2. Synthesis of 2,3-Bis(hexadecyloxy)-5,12-diphenyltetracene (G).** 2,3-Bis(hexadecyloxy)tetracene-5,12-dione was synthesized according to the literature procedures.[22] 2,3-Bis(hexadecyloxy)tetra-5,12-quinone (200 mg, $2.71 \times 10^{-4}$ mol) was suspended in 30 mL of THF under argon and cooled in an ice bath. A 1.36 mL volume of phenylmagnesium bromide (1.0 M in THF) was added dropwise. The reaction was stirred for 1 h at 0 °C, allowed to reach room temperature, and stirred for another 48 h. Afterward, the reaction was added to 150 mL of water and extracted with diethyl ether. The organic layer was dried over $MgSO_4$, and the solvent was removed in vacuo. The residue was dissolved in 20 mL of diethyl ether, protected from light, and heated to reflux. A 4 mL volume of HI (57% in water) was added dropwise under reflux and the mixture stirred at reflux for another 20 min. The reaction was allowed to cool, added to a 10% $Na_2S_2O_5$ solution, and extracted with diethyl ether. The organic layer was dried over $MgSO_4$, and the solvent was evaporated. The product was isolated by column chromatography on silica gel (eluent dichloromethane (DCM)/petroleum ether, 1:4) Yield: 37%. To obtain the product in a solid state, it can be crystallized from DCM/MeOH. $^1$H NMR ($CDCl_3$, 300 MHz): $\delta$ (ppm) = 0.87 (t, $^3J$ = 6.7 Hz, 6 H, $CH_3$), 1.2−1.4 (m, 52 H, $CH_2$), 1.75 (m, 4 H, $CH_2$), 3.85 (t, $^3J$ = 6.5 Hz, 4 H, $OCH_2$), 6.79 (s, 2 H, ArH), 7.25 (m, 2 H, ArH), 7.5−7.7 (m, 10 H, ArH), 7.75 (m, 2 H, ArH), 8.19 (s, 2 H, ArH). $^{13}$C NMR ($CDCl_3$, 300 MHz): $\delta$ (ppm) = 14.12 ($CH_3$), 22.69, 26.00, 28.69, 29.37, 29.41, 29.63, 29.67, 29.73, 31.93 ($CH_2$), 68.35 ($OCH_2$), 104.36 ($C_{Ar}H$), 124.62 ($C_{Ar}H$), 124.83 ($C_{Ar}H$), 126.96 ($C_{Ar,q}$), 127.42 ($C_{Ar}H$), 128.29 ($C_{Ar}H$), 128.55 ($C_{Ar,q}$), 128.62 ($C_{Ar}H$), 130.38 ($C_{Ar,q}$), 131.42 ($C_{Ar}H$), 134.05 ($C_{Ar,q}$), 139.85 ($C_{Ar,q}$), 149.49 ($C_{Ar,q}$). Note that not all signals of the $CH_2$ groups are visible due to overlapping. HRMS (ESI, positive ions): *m*/*z* calcd for $[C_{62}H_{84}O_2]^+$ 860.6465, measd 860.6471.

**3. Synthesis of 2,3-Bis(hexadecyloxy)-5,6,11,12-tetraphenyltetracene (R).** 2,3-Dimethoxy-6,11-diphenyltetracene-5,12-dione was synthesized according to the literature procedures.[23] 2,3-Bis(hexadecyloxy)-6,11-diphenyltetracene-5,12-dione was synthesized according to the following procedure: 2,3-Dimethoxy-6,11-diphenyltetracene-5,12-dione (190 mg, $4.04 \times 10^{-4}$ mol) was dissolved in 10 mL of DCM under argon and cooled in an ice bath. $BBr_3$ (1 mL of a 1 M solution in DCM, $9.7 \times 10^{-4}$ mol) was added dropwise and the reaction stirred for 30 min at 0 °C, for 1.5 h at room temperature, and finally for 2 h under reflux and was allowed to cool. The reaction was added to water, and a few drops of concentrated hydrochloric acid were added. The product was extracted with diethyl ether, and the organic phase was washed with water and brine and dried over $MgSO_4$, and the solvent was removed in vacuo. The residue was dissolved in 15 mL of DMF under argon, and potassium carbonate (0.5 g, 3.62 mmol) was added followed by 1-bromohexadecane (290 mg, $9.48 \times 10^{-4}$ mol). The reaction was stirred at 130 °C for 14−15 h. The solvent was removed in vacuo, and the residue was absorbed on silica gel. The product was isolated by column chromatography on silica gel (eluent DCM/petroleum ether, 1:1). Yield: 33%. $^1$H NMR ($CDCl_3$, 300 MHz): $\delta$ (ppm) = 0.87 (t, $^3J$ = 6.4 Hz, 6 H, $CH_3$), 1.2−1.5 (m, 52 H, $CH_2$), 1.82 (m, 4 H, $CH_2$), 4.03 (t, $^3J$ = 6.6 Hz, 4 H, $OCH_2$), 7.28−7.34 (m, 4 H, ArH), 7.42−7.64 (m, 12 H, ArH). 2,3-Bis(hexadecyloxy)-6,11-diphenyltetracene-5,12-dione (385 mg, $4.32 \times 10^{-4}$ mol) was dissolved in 10 mL of THF under argon and cooled in an ice bath. A 1.2 mL volume of PhLi (1.8 M in dibutyl

(33) The dry fibers are more exposed to residual and detrimental oxygen than the previously degassed DMSO gels, impeding more detailed investigations of this system under the current microscopy setup.

(34) (a) Prasanthkumar, S.; Saeki, A.; Seki, S.; Ajayaghosh, A. *J. Am. Chem. Soc.* **2010**, *132*, 8866. (b) Hong, J.-P.; Um, M.-C.; Nam, S.-R.; Hong, J.-I.; Lee, S. *Chem. Commun.* **2009**, 310.

(35) Giansante, C.; Olive, A. G. L.; Schäfer, C.; Raffy, G.; Del Guerzo, A. *Anal. Bioanal. Chem.* **2010**, *396*, 125.

(36) (a) Shklyarevskiy, I. O.; Jonkheijm, P.; Christianen, P. C. M.; Schenning, A. P. H. J.; Del Guerzo, A.; Desvergne, J.-P.; Meijer, E. W.; Maan, J. C. *Langmuir* **2005**, *21*, 2108. (b) Hung, A. M.; Stupp, S. I. *Langmuir* **2009**, *25*, 7084. (c) Hirai, Y.; Babu, S. S.; Praveen, V. K.; Yasuda, T.; Ajayaghosh, A.; Kato, T. *Adv. Mater.* **2009**, *21*, 4029.

ether) was added dropwise and the reaction stirred in the melting ice bath overnight. Afterward, the solution was added to a saturated $NH_4Cl$ solution and extracted with diethyl ether twice. The combined organic phases were washed with water and dried over $MgSO_4$, and the solvent was evaporated. The residue was dissolved in diethyl ether, protected from light, and refluxed. A 6 mL volume of HI (57% in water) was added slowly under reflux, which was continued for another 25 min. Afterward, the reaction was allowed to cool, added to a 10% $Na_2S_2O_5$ solution, and extracted with diethyl ether. The organic phase was washed with water and dried over $MgSO_4$, and the solvent was removed in vacuo. The product was isolated by column chromatography on silica gel (eluent DCM/petroleum ether, 1:4). Yield: 34% of a red oil. To obtain the product in a solid state, it can be crystallized from DCM/MeOH to give a red-orange powder. $^1$H NMR (THF-$d_8$, 300 MHz): $\delta$ (ppm) = 0.89 (t, $^3J$ = 6.8 Hz, 6 H, $CH_3$), 1.2−1.4 (m, 52 H, $CH_2$), 1.64 (m, 4 H, $CH_2$), 3.65 (t, $^3J$ = 6.3 Hz, 4 H, $OCH_2$), 6.51 (s, 2 H, ArH), 6.82−6.88 (m, 8 H, ArH), 6.98−7.12 (m, 14 H, ArH), 7.31 (m, 2 H, ArH). $^{13}$C NMR (THF-$d_8$, 200 MHz): $\delta$ (ppm) = 14.66 ($CH_3$), 23.76, 27.14, 29.89, 30.51, 30.79, 30.87, 33.07 ($CH_2$), 68.82 ($OCH_2$), 104.88 ($C_{Ar}H$), 125.20 ($C_{Ar}H$), 126.59 ($C_{Ar}H$), 126.64 ($C_{Ar}H$), 127.39 ($C_{Ar}H$), 128.19 ($C_{Ar}H$), 128.38 ($C_{Ar}H$), 129.47 ($C_{Ar,q}$), 129.51 ($C_{Ar,q}$), 131.02 ($C_{Ar,q}$), 133.15 ($C_{Ar}H$), 133.36 ($C_{Ar}H$), 135.11 ($C_{Ar,q}$), 137.27 ($C_{Ar,q}$), 143.37 ($C_{Ar,q}$), 143.80 ($C_{Ar,q}$), 151.08 ($C_{Ar,q}$). Note that not all signals of the $CH_2$ groups are visible due to overlapping. HRMS (ESI, positive ions): $m/z$ calcd for $[C_{74}H_{92}O_2]^+$ 1012.7091, measd 1012.7101.

**Confocal Fluorescence Microscopy.** The samples were prepared using deoxygenated solvents and then placed under a continuous light $N_2$ gas flow. We used a Picoquant Microtime 200 with two MPD SPADs and a Ti−Sa laser chain (Coherent) yielding 4−6 ps pulses at 4.75 MHz. An 80% T/20% R spectrally flat beam splitter was used in combination with a microscope objective (100× UPLSAPO, NA 1.4), suitable interferential filters, a 50 $\mu$m pinhole, and, when specified, a polarizing beam splitter and two Glan-Thompson polarizers. For polarization microscopy, the instrumental $G$-factor was measured for each spectral range with a crystal (2,3-bis(heptyloxy)anthracene, 400−450 nm) or a solution of **G**, **R**, or **G** + **R** (500−700 nm). Typical laser powers of ∼30 W/cm$^2$ at 385 nm and ∼130 W/cm$^2$ have been used. Spectroscopy was performed with an Andor system, collecting after the pinhole. A distance of 250 nm between each pixel and an acquisition time of 0.6 ms per pixel have been used, and each spectrum is the sum of the fluorescence of 20 pixels. The spectra were intensity corrected for instrumental response, measuring suitable reference solutions that cover the whole spectral range. FLIM results were obtained using the Symphotime fitting software, which performs a multiexponential fitting (one, two, or three exponentials depending on the sample) at each pixel. In Figure 6a,b, the color codes represent the average lifetime resulting from a triexponential fitting. Figure 6d: the color codes represent the value of the monoexponential decay time. In Figure 6e′,e″, the color codes represent the rise time (5, e′) and the decay time (5, e″) resulting from biexponential transient emission (a triexponential fitting by FLIM, with two short rise times and one long decay time, is difficult because the long decay component has by far the highest contribution to emission). Parts c and f of Figure 6 are histograms of photons counted for each occurrence of a determined decay time: when the fitting is triexponential using $\sum A_i \exp(-t/\tau_i)$, the counts of each pixel are divided into three weighted contributions, $A_1\tau_1/\sum A_i\tau_i$, $A_2\tau_2/\sum A_i\tau_i$, and $A_3\tau_3/\sum A_i\tau_i$.

**Fluorescence.** Bulk fluorescence spectra were obtained on a Horiba Jobin-Yvon Fluorolog spectrofluorimeter. Fluorescence quantum yields of **G** and **R** were determined in deoxygenated THF using as a reference fluorescein at pH 11.[25] A Labsphere optical Spectralon integrating sphere (diameter 100 mm), which provides a reflectance of >99% over the 400−1500 nm range, has been used to measure quantum yields of deoxygenated **B**- and **W**-gels (light intensity measured, not power).[25]

**Acknowledgment.** We thank M. Cantuel and N. McClenaghan. Financial support was provided by Project ANR-06-JCJC-0030, Région Aquitaine (Ph.D. fellowship to M.-T.K.; equipment, Grant 20051304008AB), GIS AMA, CNRS, and the French Ministry of Education and Research.

**Supporting Information Available:** Synthesis, structures, and additional spectra. This material is available free of charge via the Internet at http://pubs.acs.org.

JA106807U